MNRAS **000**, 1–8 (2018) Preprint 24 August 2018 Compiled using MNRAS LATEX style file v3.0

Discovery of s-process enhanced stars in the LAMOST survey

Brodie. J. Norfolk,[1]★† Andrew. R. Casey[1,2], Matthew T. Miles[1], Alex J. Kemp[1], Amanda I. Karakas[1], Kevin C. Schlaufman[4], Melissa Ness[5], Anna Y. Q. Ho[3], John C. Lattanzio[1], Alexander P. Ji[6]

[1]*School of Physics & Astronomy, Monash University, Clayton 3800, Victoria, Australia*
[2]*Faculty of Information Technology, Monash University, Clayton 3800, Victoria, Australia*
[3]*Cahill Center for Astrophysics, California Institute of Technology, MC 249-17, 1200 E California Blvd, Pasadena, Ca, 91125, USA*
[4]*Department of Physics and Astronomy, Johns Hopkins University, 3400 N Charles St., Baltimore, MD 21218, USA*
[5]*Department of Astronomy, Columbia University, 550 West 120th Street New York, New York 10027*
[6]*Carnegie Observatories*

Accepted XXX. Received YYY; in original form ZZZ

ABSTRACT

Here we present the discovery of 895 stars enriched in s-process elements from the LAMOST spectra using a data-driven approach. This sample constitutes the largest number of s-process enhanced stars ever discovered. Our sample includes; 187 s-process candidates that are enhanced in both barium and strontium, 49 stars with significant barium enhancement only, and 659 stars that show only strontium enhancement. Our entire s-process candidate sample exists within temperature and luminosity ranges not enveloped by the AGB?, which may indicate a recent (< 1 Myr) mass accretion event from an AGB companion. The majority of our barium stars (95%) show strong carbon enhancements yet, only 5 candidates (< 3 %) show evidence of sodium enhancement, in tension with previous observations of enhanced Na among s-process candidates. We argue this may have been a selection bias? in previous studies. Our kinematical analysis reveals our sample is composed of 97% disk stars, and 3% with velocity consistent to the halo. A comparison with AGB yields suggests the main neutron source responsible for Ba and Sr enhancements is the $C^{13}(\alpha,n)O^{16}$ reaction chain. Theoretical models show that this source is dominant in low-mass AGB stars. We conclude that the progenitors for s-process enhancement in our sample are AGB companion stars with masses $1-3\,M_{\odot}$.

Key words: stars: chemically peculiar – stars: abundances

1 INTRODUCTION

The abundance of elements created through the slow neutron-capture process (s-process), is a measure of the nucleosynthetic reactions that occur primarily in Asymptotic Giant Branch (AGB) stars. Due to their associated enrichment of the s-process element barium, stars with peculiar enhancements of carbon, and heavy elements (Z > 30) are commonly referred to as 'barium stars' (Bidelman & Keenan 1951). The naming convention associated with 'barium stars' is historical, for the purposes of this paper it is necessary to classify definitions used for subsequent discussions. Stars with Ba and Sr enrichment will be refereed to as s-process candidates, and singular enhancement samples will be named according to their respective element. Metallicity-dependent classifications also exist in the literature. Metal-poor stars ([Fe/H] ≈ [0,-1.2]) enriched by s-process elements are classically refereed to as CH stars, we will simply define them as metal poor s-process candidates. An abundance criteria may also be used to define s-process enrichment, this is typically taken as threshold of [Ba/Fe] ≥ +0.3 (Malaney & Lambert 1988). For the purposes of this paper, s-process enrichment will be determined solely on the presence significant flux residuals as described in Section 2.1.2. S-process candidates can be classified as either extrinsic or intrinsic objects. Extrinsic s-process stars are stellar phenomena exhibiting an enhancement as the result of some polluting process. Stars intrinsically enhanced in s-process elements are known as AGB S stars. These stars are in the TP-AGB (thermally pulsing-asymptotic giant branch) phase. During this stage of nucleosynthesis, the s-process produces an over-abundance of both carbon and heavy elements. The thermal pulsing cycle transports these elements to surface of TP-AGB stars. According to the mass-transfer hypothesis, extrinsic s-process stars are a consequence of stellar wind accretion

★ E-mail: bjee7@student.monash.edu (MU)
† This paper includes data gathered with the 6.5 meter Magellan Telescopes located at Las Campanas Observatory, Chile.

(Boffin & Jorissen 1988; Jorissen & Boffin 1992) or Roche-lobe overflow (Webbink 1986). Both dynamical systems require a binary configuration with a previous TP-AGB companion star (AGB S star) in its final phase as a white dwarf (Böhm-Vitense 1980; Böhm-Vitense et al. 1984). In fact, McClure (1983) determined 85% of all s-process candidates are in binary systems. They further claimed that stars which appeared to be singular are actually pole-on, or highly eccentric binaries with significant radial velocity variations only occurring in a small ranges (Pourbaix et al. 2004). For these reasons, the properties and occurrence rate of s-process candidates are informative of the binary star fraction as a function of metallicity, the mass ratio of binary stars, as well as AGB yields across different masses and metallicities.

Occurring in the interior of AGB stars, the s-process synthesises roughly half of all elements heavier than iron (e.g., Busso et al. 1999; Travaglio et al. 2001; Herwig 2005; Bisterzo et al. 2014; Karakas & Lattanzio 2014). During the subsequent TP-AGB phase, thermal instabilities occur in the He shell every 10^5 years or so, depending on the mass of the H-exhausted core. These energy bursts drive a convective zone that sweeps almost the entire region lying between the core and the He-shell, mixing the products of nucleosynthesis within these regions. While simultaneously, forcing the star to expand and pushing the H-shell out to cooler regions (Karakas et al. 2002). The convective envelope will then move inwards towards regions previously mixed by the thermal pulse driven convective zones. This phase of expansion and resulting inward movement is defined as the third dredge up (TDU), and is theorised to occur after each thermal pulse. During the TP-AGB phase, the TDU is responsible for the surface enrichment in ^{12}C and heavy elements produced by the s-process (e.g., Busso et al. 2001). Post dredge up the star contracts, reigniting the H-shell, and producing the majority of the surface luminosity for the next interpulse period. The interpulse, thermal pulse, and dredge up cycle may occur numerous times and the frequency depends on the initial mass, composition, and mass-loss rate of the star.

S-process candidate can form within a metallicity-dependent initial mass range of approximately $0.8-8\,M_{\odot}$ (Karakas et al. 2016). The minimum mass is defined by the onset of core helium burning, and the maximum by core carbon burning. The age of these stars varies considerably, with some reaching ages ≈ 12 Gyr in metal-poor globular clusters. Less massive metal-rich stars may reach ages of $\approx$ 100Myr, this includes stars that are at the core carbon burning limit or very close to it (e.g., Whitelock et al. 2013). The majority s-process candidates are observed to be members of the disk (Jorissen et al. 1993; Gomez et al. 1997; Mennessier et al. 1997). In Pereira et al. (2011), it is shown that metal-rich s-process candidates share similar kinematics to other metal-rich and super metal-rich stars already analysed, suggesting that they do not belong to the bulge population. Jorissen et al. (1993) relates galactic position to the extrinsic or intrinsic nature of the s-process candidate. They show that intrinsically enhanced stars are more concentrated towards the galactic plane than extrinsic enhanced stars.

In this paper we analyse 454,180 giant stars from the second LAMOST data release (Luo et al 2015) and identify 895 s-process candidates. In Section 2 we describe the observations and candidate selection. Section 3 details the analysis of high-resolution follow-up observations obtained for a few candidates. In Section 4 we discuss the properties of our s-process candidates in context of existing literature. We provide concluding remarks in Section 5.

2 METHODS

2.1 LAMOST analysis

2.1.1 *Data-driven analysis*

The LAMOST (Large sky Area Multi-Object Fibre Spectrographic) survey released low-resolution ($\mathcal{R} \approx 1800$) optical spectra (3700 Å to 9000 Å) for 2,207,189 stars in their second data release (Luo et al 2015). Stellar parameters ($T_{\rm eff}$, $\log g$, [M/H], [α/M]) were derived by (Ho et al. 2017) using a *The Cannon* Ness et al. (2016), with labels for 9,952 giant stars in common between LAMOST and the APOGEE survey. We note that this sample is limited to giant stars, implying that we would not identify dwarf s-process enhanced stars. Cross-validation tests shows that the typical uncertainties are approximately 70 K in effective temperature $T_{\rm eff}$, 0.1 dex in surface gravity $\log g$, 0.1 dex in metallicity [M/H], and 0.04 dex in the α-element abundance relative to overall metallicity [α/M]. These uncertainties are comparable to the those present in APOGEE (Alam et al. 2015).

2.1.2 *Candidate selection*

The s-process candidates in this work were identified by filtering for significant flux residuals. We fit a Gaussian distribution with amplitude A to the flux residuals at each s-process element absorption line. These included; 4554 Å (Ba II) and 4077 Å (Sr II) wavelengths for s-process candidates, 4554 Å (Ba II) and 4934 Å (Ba II) wavelengths for barium enriched candidates, and wavelengths at 4077 Å (Sr II) and 4215 Å (Sr II) for strontium enriched candidates. The amplitude of each Gaussian fit at each wavelength is analogous to the depth of each absorption line. The discrepancy is then measured as the difference between the normalised LAMOST flux and the data driven model. A negative residual indicates enrichment, this is shown for a randomly chosen s-process candidate in Figure 1. We used five filters for each spectrum and subsequent set of absorption lines in order to identify s-process enrichment, these included:

(i) Profile amplitude for both enhancement lines must be $A < -0.05$, indicating a stronger absorption line than expected by the model.
(ii) Both amplitudes must be measured within 3σ ($|A|/\sigma_A < 3$).
(iii) The wavelength at each absorption line must be within 2 Å ($\lambda < 2$) of the rest frame laboratory model.
(iv) The reduced χ^2 from *The Cannon* must be $\chi^2_r < 3$.
(v) The LAMOST spectra must have a signal-to-noise ratio of $S/N > 30\,\mathrm{pixel}^{-1}$.

We use visual inspection with all candidates to exclude any results containing false positives: candidates with data reduction issues; apparent absorption finer then the spectral resolution; or overly noisy normalised LAMOST spectra. This approach discovers 895 s-process rich candidates which are provided in Table 1. This sample consists of; 187 s-process candidates, 49 barium enriched stars, and 659 stars with strontium enrichment. It is the largest collection of s-process enhanced stars ever discovered, with the next sample of significant size containing 182 s-process candidates (e.g., deCastro et al. 2016).

For the remainder of this paper we restrict our analysis to the 187 s-process candidates that show enhancement in both barium and strontium. While the 49 or 659 stars with only barium or strontium enhancements (respectively) may also be classified as s-process

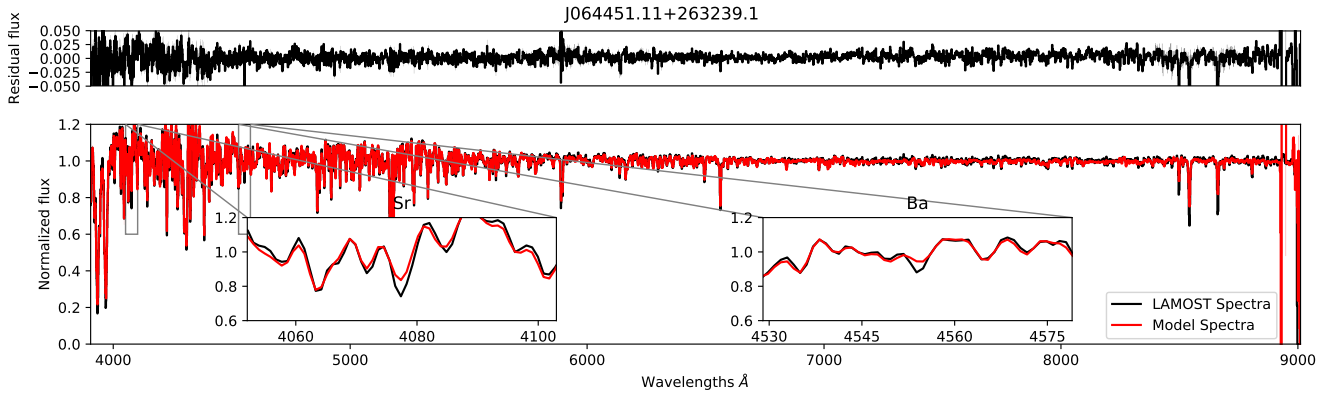

Figure 1. Pseudo-continuum-normalised LAMOST spectra for the s-process candidate J064451.11+263239.2. The data are shown in black and the best-fitting data-driven model is shown in red. We include zoom-in axes to show significant deviations in Sr and Ba at 4077 Å and 4554 Å respectively.

candidates, there may be other explanations for their chemical abundance pattern (e.g., Maiorca et al. 2011).

2.1.3 *Enhancements due to sodium, technetium, and carbon*

Enhancements in sodium, technetium, and carbon are useful indicators when determining whether a sample is populated by intrinsically enhanced AGB S stars, or polluted extrinsic barium stars. We? performed an identical analysis to the process described in Section 2.1.2 in order to identify sodium, technetium, or carbon enhancement in our sample of 187 s-process candidates. For sodium enrichment, we required significant absorption in the doublet lines at 5889 Å and 5895 ÅÒnly 5/187 s-process candidates met this criteria. For technetium enhancement, we searched for significant residual deviations at 4049 Å, 4238 Å, 4262 Å, 4297 Å, and 5924 Å. These absorption lines are extremely weak, and would require a substantial amount of technetium enhancement before it would be visible in a high S/N LAMOST spectrum. We found that 51 s-process candidates exhibited some level of significant enhancement at the single absorption line 4238 Å. Single line enrichment discovered by our data driven approach are very likely attributed to data reduction/calibration artefacts present. These artefacts exist within in our data as a result of fitting a model to the LAMOST spectral data. As such, the 51 stars enhanced in a single Tc line can be ruled out as false positives. For carbon enhancement we searched for significant deviations at the CH and G band near 4300 Å, of which 178/187 s-process candidates exhibited significant carbon enhancement (i.e., [C/Fe] $\gtrsim$ 0.5).

2.1.4 *Abundances estimated from LAMOST spectra*

We estimated [Ba/Fe] and [Sr/Fe] abundance ratios for all s-process enhanced candidates by synthesising spectra. We assumed that absorption due to metals is captured by *The Cannon* model, and deviations in flux at the 4554 Å Ba II line and the 4077 Å Sr II transition are solely due to enhancements in Ba and Sr, respectively. We used an extensive grid of model atmospheres developed by the MARCS program (Gustafsson et al. 2008), determined stellar parameters using the SME code(Valenti & Piskunov 1996),?

In analyses of stellar spectra and colours, and for the analysis of integrated light from galaxies, a homogeneous grid of model atmospheres of late-type stars and corresponding flux spectra is needed We construct an extensive grid of spherically-symmetric models (supplemented with plane-parallel ones for the highest surface gravities), built on up-to-date atomic and molecular data, and make it available for public use.

(Gustafsson et al. 2008; Valenti & Piskunov 1996; Kupka et al. 1999; Blanco-Cuaresma et al. 2014). We adopted the stellar parameters ($T_{\rm eff}$, log g, [Fe/H]) from Ho et al. (2017), and assume a microturbulence of v_{mic} = 2 km s^{-1}. Uncertainties in [Ba/Fe] and [Sr/Fe] from LAMOST are taken as the fitting error due to noise, added in quadrature with an adopted 0.2 dex systematic error floor.

Our analysis shows 186/187 of our s-process candidates exhibit enhancement at the BaII resonance line 4554 with a [Ba/Fe] $\geq$ +0.3, and a average abundance error of 0.1. Previous studies Malaney & Lambert (1988) have defined s-process candidates through an abundance criteria of [Ba/Fe] $\geq$ +0.3. Using this measure, only one star (J092155.95 + 265253.4) from our sample exhibits a lower [Ba/Fe] of 0.12. This however does not rule out s-process enhancement for this candidate. As previously discussed, a negative residual at the Ba II resonance line 4554 Å indicates s-process enhancement and as discussed in section 2.1.3, carbon enrichment is observed frequently with s-process enhancement. J092155.95+265253.4 shows both a negative residual at 4554 Å and carbon enrichment, we therefore conclude that this single deviant case can be classified as a s-process candidate. This additionally applies to candidates that fall under [Ba/Fe] $\geq$ +0.3 due to the average abundance error.

2.2 Dynamics

We integrated the galactic orbits using recent astrometry from Gaia (Gaia Collaboration et al. 2016, 2018b; Cropper et al. 2018; Katz et al. 2018; Lindegren et al. 2018; Sartoretti et al. 2018) for 871/895 s-process enhanced stars with parallax > 0 and parallax/parallax error > 5 selection filters. We integrated each star backwards for 0.5 Gyr using the `gala` Python package (Price-Whelan 2017) in a Milky Way-like potential (Price-Whelan 2014) that consists of four components: a Hernquist (1990) bulge and nucleus, a Miyamoto-Nagai (1975) disk, and a Navarro, Frenk & White (1997) halo. We computed spatial velocities relative to the local standard of rest, where U_{LSR} is positive towards the Galactic centre, V_{LSR} is positive in the direction of Galactic rotation (l = 90°, b = 0°), and W_{LSR} is positive towards the north galactic pole (b = 90°). Our

Table 1. Properties of 895 s-process candidates, the table is available online in its entirety. Here we show a portion to demonstrate its style and content.

2MASSID	R. A. (J2000)	Dec. (J2000)	v_r (km s^{-1})	S/N (pixel^{-1})	$T_{\rm eff}$ (K)	log g	[Fe/H]	[α/Fe]	χ^2_r	[Ba/Fe]	[Sr/Fe]	Ba II	Sr II	Ba II & Sr II
J000019.26+501444.8	00:00:19.27	+50:14:44.9	-3.9	49	4973	3.27	0.21	0.08	0.66	0.25	0.83	✗	✓	✗
J000020.55+411348.1	00:00:20.56	+41:13:48.2	-28.2	32	4882	2.74	-0.22	0.04	0.23	-0.17	0.90	✗	✓	✗
J000134.95+490743.2	00:01:34.96	+49:07:43.2	-42.3	72	5044	3.11	-0.54	0.11	0.79	1.02	0.45	✗	✗	✓
J000258.09+410730.0	00:02:58.10	+41:07:30.1	-34.5	41	4697	2.57	-0.22	0.12	0.98	-0.10	0.80	✗	✓	✗
J000403.80+160257.1	00:04:03.80	+16:02:57.2	-35.4	42	5200	3.40	-0.41	0.09	0.33	0.92	0.52	✗	✗	✓
J000439.16+183350.3	00:04:39.17	+18:33:50.4	-38.7	31	4601	2.50	0.44	0.03	0.34	-0.11	0.88	✗	✓	✗
J000444.87+400402.1	00:04:44.88	+40:04:02.1	-94.7	53	4172	1.46	-0.08	0.09	0.72	0.03	0.91	✗	✓	✗
J000552.76+261849.3	00:05:52.76	+26:18:49.4	-22.5	73	4924	3.14	-0.05	0.09	0.67	0.28	0.85	✗	✓	✗
J000737.70+394055.5	00:07:37.70	+39:40:55.6	-31.5	33	4700	2.80	-0.04	0.07	0.28	-0.13	0.81	✗	✓	✗

analysis revealed 97% disk star membership and 3% with velocity consistent to the halo which is shown using a Toomre diagram in Figure 4.

3 FOLLOW-UP OBSERVATIONS WITH MAGELLAN/MIKE

3.1 Observations and data reduction

On 07 January 2018 we acquired a high-resolution spectrum of two s-process candidates (J09162834+0259348 and J08351472-0548480) using the MIKE (Magellan Inamori Kyocera Echelle) (Bernstein et al. 2003) spectrograph on the Magellan Clay telescope (Schectman & Johns 2003) at Las Campanas Observatory, Chile. Candidates were observed as part of another program not a detailed follow-up campaign. They were chosen based on observability constraints and ranked by their apparent visual magnitude, with both candidates having $V \approx 12$. We observed both stars in good seeing using the 0.7 arcsecond slit and 2x2 spatial on-chip binning, providing a spectral resolution of $\mathcal{R} \approx 28,000$. Exposure times of 100 seconds were sufficient to achieve a S/N ratio exceeding 30 per pixel at 4500 Å. We acquired calibration (biases, milky, quartz, and Th-Ar arc lamp) frames in the afternoon. We reduced the data using the `CarPy` package (Kelson et al. 2000). We used spline functions to continuum-normalise all echelle orders, and resampled the normalised spectra onto a uniform-spaced wavelength map. We used a rest-frame normalised template of a FGK-type star to place the observed spectra at rest.

3.2 Abundance analysis

We adopted the stellar parameters ($T_{\rm eff}$, $\log_{10} g$, [Fe/H]) provided from the data-driven analysis of Ho et al. (2017). Following the procedure outlined in Casey (2014), we measured the strength of Ba II (4554 Å, 4934 Å, and 6496 Å) and Sr II (4077 Å and 4215 Å) absorption lines by spectral synthesis, using s-process isotopic ratios from Sneden et al. (2008). The abundance ratios we estimate from high-resolution spectra are in excellent agreement with our estimates from LAMOST spectra, all agreeing within the joint 1.2σ. Specifically, for J09162834+02593480 from high- and low-resolution spectra, respectively, we find [Sr/Fe] = 0.76 ± 0.10 and 0.85 ± 0.21, and [Ba/Fe] = 0.92 ± 0.10 and 0.77 ± 0.21. The biggest discrepancy we find between high- and low-resolution spectra is [Sr/Fe] for J09162834+0259348, where we find [Sr/Fe] = 0.62 ± 0.07 from our Magellan/MIKE spectra, and 0.90 ± 0.22 from LAMOST. Finally, for J09162834+0259348 we find [Ba/Fe] = 0.94 ± 0.12 from high-resolution spectra and [Ba/Fe] = 0.80 ± 0.26 from low-resolution spectra. Uncertainties on abundances derived from high-resolution spectra are taken as the standard deviation of multiple line measurements. The high-resolution abundances we find help validate our methodology for candidate selection, and for estimating abundances from LAMOST spectra.

4 DISCUSSION

4.1 Extrinsic or intrinsic

Barium enhanced stars exist as either intrinsic or extrinsic stellar objects. Intrinsically enhanced barium stars must be massive enough to reach the TP-AGB phase, and extrinsic barium stars must be in a binary with a previously polluting TP-AGB star companion (AGB S star). Figure 2 shows that the majority of our stellar sample exists within temperature and luminosity ranges not enveloped by the AGB. This highlights that our sample does not contain stars to the degree of evolution required to reach the TP-AGB phase, and therefore, must be extrinsic barium stars. However, stars with temperatures below 3800K in Figure 2 are potential AGB stars, and their intrinsic or extrinsic nature is not certain. Additionally, it's important to note, previous literature (Van der Swaelmen et al. 2017), state only 33% of their stellar sample are post-main-sequence barium stars (extrinsic barium stars). In comparison, we find that all our barium candidates to be extrinsic. This suggests, the construction of our data-driven model may have missed some AGB barium candidates, or that previous studies were biased towards finding luminous AGB S stars. Given that our analysis limits us to only giant stars, such that we do not find any extrinsic barium stars on the main-sequence, naïvely we would expect that our sample would be biased *towards* finding a higher fraction of red giant stars. Given this bias, Figure 3 illustrates through the temperature, and log g ranges present, that our sample is exclusively populated by red giant extrinsic barium stars. This suggests unaccounted selection biases in previous studies towards luminous AGB S stars.

4.2 Sodium enhancement

Sodium overabundances observed in the atmospheres of giants is thought to be synthesised by the NeNa reaction chain in the convective core of main-sequence stars (El Eid & Champagne 1995). Sodium is transported to the surface of these giants via mixing during the first dredge-up, and stars with a minimum mass of 1.5 $M_\odot$ can exhibit enhanced sodium abundances through the NeNa cycle (Denissenkov & Ivanov 1987; Smiljanic 2012). Antipova et al. (2004) reported sodium enhancements in 3 of their 16 barium star candidates, and they relate this to the dredge-up of nuclear-burning material produced by convection during the red-giant phase. Moreover, they suggest that [Na/Fe] ratios are systematically higher for giants with lower log g values, however, these [Na/Fe] ratios do not exhibit variations in metallicity. Similarly, deCastro et al. (2016)

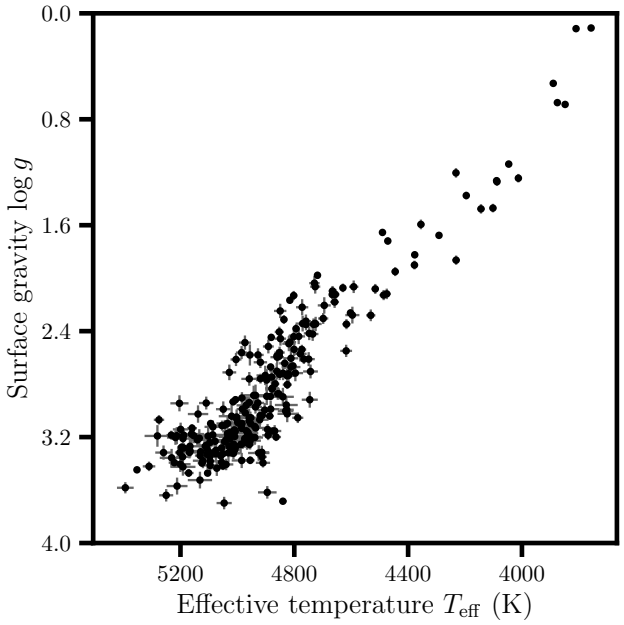

Figure 2. Effective temperature $T_{\rm eff}$ and surface gravity $\log g$ for 257 candidate barium stars from LAMOST.

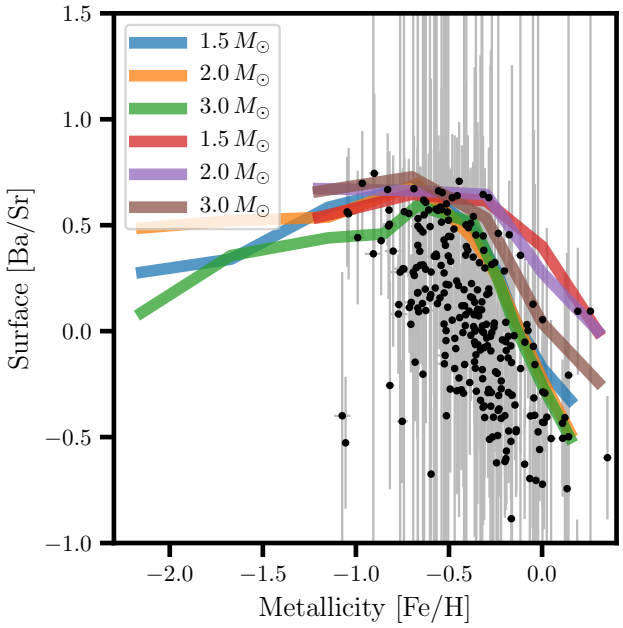

Figure 3. Metallicities ([Fe/H]; x-axis) and heavy-to-light s-process abundance ratios ([Ba/Sr] as measured from LAMOST; y-axis) for 187 barium star candidates. Coloured lines blue, orange, and green, indicate surface [hs/ls] yields from Cristallo et al. (2015) for different masses. Coloured lines red, purple, and brown indicate surface [hs/ls] yields from Karakas & Lugaro (2016) for [Fe/H] at +0.3. 0.0, and -0.3. From Karakas (2018) for [Fe/H] at -0.7, and from Fishlock et al (2014) for [Fe/H] at -1.2.

highlights the possible weak anti-correlation between [Na/Fe] ratio and $\log g$, and highlights that this trend is present in previous studies (e.g., Boyarchuk et al. 2002; Mishenina et al. 2006; Luck & Heiter 2007; Takeda et al. 2008).

We find that $< 2\,\%$ of our barium stars show sodium enhancement, contrary to previous studies (e.g., deCastro et al. 2016), indicating all s-process enhanced stars will exhibit Na enhancement. We also note that the 5 sodium-enhanced barium stars all have values of, $\log g \approx 3$, which is inconsistent with the literature. Previous studies suggest, lower $\log g$ values are expected, given low $\log g$ values systematically contribute to higher [Na/Fe] abundance ratios. It is important to note, sodium enhancement can occur due to the presence of interstellar dust. Using the IRSA's all-sky dust map (Schlafly & Finkbeiner 2011), we find that 2 of 5 of these stars have E(B-V)≈ 0.35, suggesting that the flux residuals around the Na doublet are due to interstellar absorption. However, 3 exhibit low (≈0.045) E(B-V) values, indicating, the enhancement is more likely due to stellar absorption. These results suggest that sodium-rich material from a companion TP-AGB star has polluted these 3 barium candidates, but more importantly, sodium enhancement is by no means ubiquitous in barium stars. However, it should be highlighted that low resolution spectra can result in Na line saturation, limiting the flux enhancement even with an abundance enhancement.

The data that led deCastro et al. (2016) to conclude that barium stars have higher [Na/Fe] ratios is subject to systematic differences (biases) between Milky Way studies of normal FGK-type stars, and those focussed on barium stars. This has the potential to contain unresolved differences in the reported [Na/Fe] abundance ratio. These systematic effects would also contribute to the observed correlation between [Na/Fe] and $\log g$, since intrinsic barium stars (by definition) have low $\log g$ values. We do not observe this correlation between [Na/Fe] and $\log g$ in our sample, and we conclude that barium stars do not have higher [Na/Fe] abundance ratios on average.

4.3 Technetium enhancement

Technetium has a half life of approximately 211,000 years and as a result, the presence of Tc enhancement is constrained to observations of AGB S stars (Jorissen et al. 1993) or recently polluted extrinsic barium stars. Our analysis, undertaken for the TC lines 4049 Å, 4238 Å, 4262 Å, 4297 Å, and 5924 Å, discovered 51 single Tc line matches at 4238,Å, within our 187 barium star candidate sample. The majority (46/51) have $\log g > 2$, suggesting they cannot be AGB S stars, and may indicate a recent (< 1 Myr) mass accretion event. However, for Tc to be present in the LAMOST spectra the enhancement must be considerably strong, and given that all 51 matches were at single lines it is concluded that these results are more likely data artefacts. In agreement with previous findings (e.g., Little-Marenin & Little 1987; Smith 1984; Smith & Wallerstein 1983), the results indicate that none of the evolved barium stars in our sample exhibited the presence of Tc enhancement, and in accordance with previous literature, it can be concluded that our barium star sample is extrinsic. However, we caution that Tc enhancement is usually a very weak signature, and the presence of Tc would require multiple lines of enhancement. Additionally, it is universally known that numerous Tc lines are considerably blended by other s-process enhancement lines (e.g., Van Eck & Jorissen 1999).

4.4 Carbon bands

Barium stars are excellent candidates for investigating the relationship between neutron-capture elements and other species that may be depleted or enhanced, since iron within these stars act as neutron seeds during the operation of the s-process. In the AGB phase the abundance of carbon is a product of helium fusion, specifically the triple-alpha process within a star. In an identical mechanism to the presence of s-process element enhancement, carbon enhanced stars exist intrinsically or extrinsically. Giants and supergiants become enhanced in carbon through TDU process discussed in Section 1, and extrinsic carbon enhancement occurs via mass transfer from a binary AGB star. Our analysis produced 178 CH and G band significantly enhanced stars (i.e., [C/Fe] $\gtrsim 0.5$) out of the total 187 barium candidates. These 178 stars exist in a metallicity range of 0 to -1.2, and can be termed "CH stars" in accordance with definitions used in the literature (e.g. Luck & Bond 1991; McClure 1997).

4.5 Comparison to AGB yields

AGB stars, and chemically unusual stars that show the chemical signature of mass transfer pollution from a binary AGB companion, highlight the variety of s-process enhancement. In Figure 3 we show the heavy-to-light s-process abundance ratio (taken as [Ba/Sr]) for all 187 barium stars identified in LAMOST. Although the [Ba/Sr] ratio is quite noisy, the overall metallicity [Fe/H] is quite precise (0.1 dex). Despite our LAMOST sample of 454,180 giants having metallicities down to about [Fe/H] = −2, we only detect barium stars down to metallicities of about [Fe/H] = −1.1. Given our barium stars exist in this metallicity range of 0 to -1.1, we can classify them as CH stars as defined in previous literature (e.g. Luck & Bond 1991; McClure 1997).

The final surface s-process index [Ba/Sr], illustrated in Figure 3, illustrates the relationship between [Ba/Sr] yields and the mass of AGB stars. This highlights the main neutron source, the $C^{13}(\alpha, n)O^{16}$ reaction chain, is responsible for the Ba and Sr enhancements. Additionally, theoretical models show that this source is dominant in low-mass AGB stars, and it follows, that most of the progenitors of s-process elements in our sample are low-mass AGB stars between $1 - 3\,M_{\odot}$. However, it's important to note, our results do not indicate when the mass transfer occurred, and our candidates fitting these theoretical yields may not have the correlating binary companion masses. Instead, mass transfer may have occurred early on in the AGB S binary companion star's lifespan, and the resulting [Ba/Sr] abundance present in our barium candidates may reflect pollution from a lower AGB S star mass. Additionally, this can be extended to our candidates not approximated by theoretical yields. Other barium candidates not fitting this relationship represent the possibly more massive, and expectedly rarer, AGB S stars within our sample.

4.6 Dynamics

The majority of our sample showed pro-grade orbits that were consistent with membership in the Milky Way disk, indicating they do not originate from an unusual stellar event. Figures 4 and 5 illustrate the galactic distribution of each class of s-process enhanced star investigated. For our entire 898 sample, Figure 4 shows 97% reside within the galactic disk (81% thin disk and 16% thick disk), and 3% within the halo. Our results show similar trends to the literature, samples from Gomez et al. (1997) and Mennessier et al. (1997) present populations of 75% contained within the disk, and 25% within the halo. Pereira et al. (2011)'s entire sample resides within the disk, and deCastro et al. (2016) states their sample contains 90% thin disk stars. Although, excluding the candidate sample presented by deCastro et al. (2016), it is important to note previous studies contain limited stellar populations ranging from 4 to 12 stars, and cannot be representative of the overall galactic distribution of s-process enhanced stars. Jorissen et al. (1993) attributes the galactic position of s-process enhanced stars as dependent on their intrinsic or extrinsic nature, given our sample is entirely extrinsic we cannot comment on the comparison between the two enhancement sources. However, given our extrinsically s-process enhanced sample concentrates towards the galactic plane, we can propose the sample in Jorissen et al. (1993) was not sufficiently large enough to represent the overarching galactic distribution of extrinsic S stars.

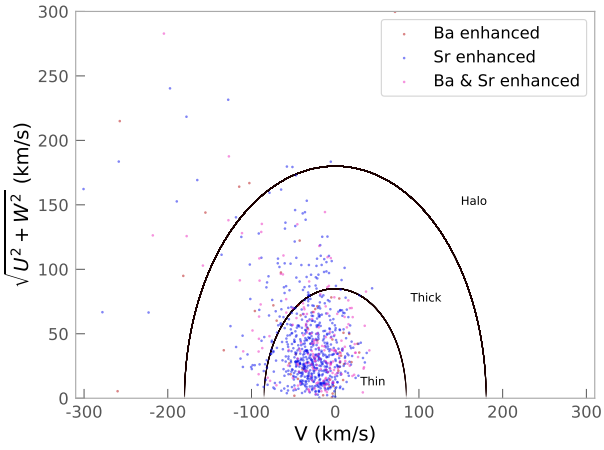

Figure 4. Galactic distribution represented by a Toomre diagram, spatial velocities ([V (km/s)]; x-axis) and ([$\sqrt{U^2 + W^2}$ (km/s)]; y-axis) for number of s-process enhanced candidates matched with Gaia DR2. Coloured markers red, blue, and purple highlight barium, strontium, and both barium and strontium enhancement respectively.

5 CONCLUSIONS

We conducted the largest ever search for s-process enhanced stars using the LAMOST second data release. From 454,180 giant stars, we identify 895 s-process candidates including: 187 stars with significant enhancements in barium and strontium (so-called 'barium stars'), 49 stars exhibiting exclusively barium enhancement, and 659 exhibiting exclusively strontium enhancement. This sample size is the greatest total number of barium stars known, and represents the largest sample of s-process enhanced stars to date. Our kinematical analysis revealed our stellar sample contains 97% disk stars (81% thin and 16% thick), and 3% halo stars, indicating our barium stars were not produced through an unusual galactic event.

We find 178/257 barium star candidates show carbon enhancement, consistent with the literature, and are possible CH stars. However, in contrast with previous works, we do not find barium stars to have significantly higher [Na/Fe] than Milky Way field giants. Only 5/257 of our barium stars show enhancement

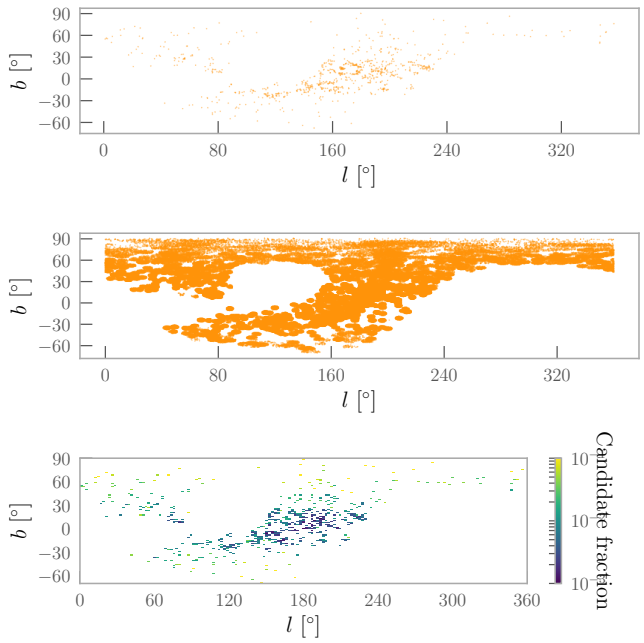

Figure 5. Galactic longitude ($[l^\circ]$; x-axis) and galactic latitude ($[b^\circ]$; y-axis) shown for: number of s-process enhanced candidates matched with Gaia DR2, the LAMOST sample matched with Gaia DR2, and a density contour between the latter two

in Na, and the flux residuals in three of those are likely due to interstellar dust. We suggest that biases between literature sources and systematic effects in measuring [Na/Fe] from stars with low $\log g$ contributed to this effect.

Despite our noisy estimates of [Ba/Fe] and [Sr/Fe] from LAMOST spectra, comparisons with AGB yields indicate the main neutron source responsible for the Ba and Sr enhancements, the $C^{13}(\alpha, n)O^{16}$ reaction chain, and theoretical yields suggest the progenitors of our s-process enhanced sample are low-mass AGB stars, between $1-3\,M_{\odot}$. We encourage follow-up observations with high-resolution spectrographs in order to precisely measure a full suite of neutron-capture abundances. This data would permit the most detailed comparisons with AGB star yields ever considered.

ACKNOWLEDGEMENTS

We thank David W. Hogg (NYU) and Hans-Walter Rix (MPIA) for useful discussions. A. R. C. is supported through an Australian Research Council Discovery Project under grant DP160100637. A. Y. Q. H. was supported by the GROWTH project funded by the National Science Foundation under PIRE Grant No 1545949, and a National Science Foundation Graduate Research Fellowship under Grant No. DGE-1144469. This research has made use of NASA's Astrophysics Data System. Guoshoujing Telescope (the Large Sky Area Multi-Object Fiber Spectroscopic Telescope LAMOST) is a National Major Scientific Project built by the Chinese Academy of Sciences. Funding for the project has been provided by the National Development and Reform Commission. LAMOST is operated and managed by the National Astronomical Observatories, Chinese Academy of Sciences. This work has made use of data from the European Space Agency (ESA) mission *Gaia* (https://www.cosmos.esa.int/gaia), processed by the *Gaia* Data Processing and Analysis Consortium (DPAC, https://www.cosmos.esa.int/web/gaia/dpac/consortium). Funding for the DPAC has been provided by national institutions, in particular the institutions participating in the *Gaia* Multilateral Agreement.

REFERENCES

Alam, S., Albareti, F. D., Allende Prieto, C., et al. 2015, ApJS, 219, 12
Antipova, L. I., Boyarchuk, A. A., Pakhomov, Yu. V.,& Panchuk, V. E. 2004, ARep, 48, 597
Bernstein, R., Shectman, S. A., Gunnels, S. M., Mochnacki, S.,& Athey, A. E. 2003, SPIE, 4841, 1694
Bidelman, W. P. & Keenan, P. C. , 1951, ApJ, 114, 473
Bisterzo, S., et al. 2014, ApJ, 787, 10 A&A, 424, 727
Blanco-Cuaresma, S., Soubiran, C., Heiter, U., & Jofré, P. 2014, A&A, 569, A111
Boffin H, M. J.,& Jorissen, A. 1988, A&A, 205, 155
Böhm-Vitense, E. 1980, ApJ, 239, L79
Böhm-Vitense, E., Nemec, J.,& Proffitt, C. 1984, ApJ, 278, 726
Bovy, J. 2015, ApJ, 216, 29
Boyarchuk, A. A., Pakhomov, Y. V., Antipova, L. I.,& Boyarchuk, M. E. 2002, ARep, 46, 819
Busso, M., Gallino, R., & Wasserburg, P. C. 1999, ARA&A, 37, 239
Busso, M., Gallino, R., Lambert, D. L., Travaglio, C.& Smith, V. V. 2001, ApJ, 557, 802
Casey, A. R. 2014, PhD Thesis, Australian National University
Cristallo, S., Straniero, O., Piersanti, L.,& Gobrecht, D. 2015, ApJ, 219, 40
Cropper, M., Katz, D., Sartoretti, P., Prusti, T., de Bruijne, J. H. J., Chassat, F., Charvet, P., Boyadijan, J., Perryman, M., Sarri, G., Gare, P., Erdmann, M., Munari, U., Zwitter, T., Wilkinson, M., Arenou, F., Vallenari, A., Gómez, A., Panuzzo, P., Seabroke, G., Allende Prieto, C., Benson, K., Marchal, O., Huckle, H., Smith, M., Dolding, C., Janßen, K., Viala, Y., Blomme, R., Baker, S., Boudreault, S., Crifo, F., Soubiran, C., Frémat, Y., Jasniewicz, G., Guerrier, A., Guy, L. P., Turon, C., Jean-Antoine-Piccolo, A., Thévenin, F., David, M. Gosset, E.,& Damerdji, Y. 2018
deCastro, D. B., Pereira, C. B., Roig, F., Jilinski, E., Drake, N. A., Chavero, C.,& Sales Silva, J. V. 2016, MNRAS, 459, 4299
Denissenkov P. A.,& Ivanov, V. V. 1987, SvAL, 13, 214
El Eid, M. F.,& Champagne, A. E. 1995, ApJ, 451, 298
Fishlock, C. K., Karakas, A. I., Lugaro, M.,& Yong, D. 2014, ApJ, 797, 44
Gaia Collaboration, Prusti, T., de Bruijne, J. H. J., Brown, A. G. A., Vallenari, A., Babusiaux, C., Bailer-Jones, C. A. L., Bastian, U., Biermann, M.,& Evans, D. W. et al. 2016, A&A, 595, A1
Gaia Collaboration, Brown, A. G. A., Vallenari, A, Prusti, T., de Bruijne, J. H. J., Babusiaux, C.,& Bailer-Jones, C. A. L. 2018,
Gustafsson, B., Edvardsson, B., Eriksson, K., et al. 2008, A&A, 486, 951
Gomez, A. E., Luri, X., Grenier, S., et al. 1997, A&A, 319, 881
Han, Z., Eggleton, P. P., Podsiadlowski, P.,& Tout, C. A. 1995, MNRAS, 277, 1443
Hernquist, L. 1990, ApJ, 356, 359
Herwig, F. 2005, ARA&A, 43, 435
Ho, A. Y. Q., Ness, M. K., Hogg, D. W., Rix, H.-W. Liu, C., Yang, F., Zhang, Y., Hou, Y.,& Wang, Y. 2017, ApJ, 836, 5
Jorissen, A.,& Boffin H, M. J., 1992, Evidences for interaction among wide binary systems: To Ba or not to Ba? In: Duquennoy, A., Mayor, M.,(eds.) Binaries as tracers of stellar formation. Cambridge Univ. Press., p.185
Jorissen, A., Frayer, D. T., Johnson, H. W., Mayor, M.,& Smith, V. V. 1993, A&A, 271, 463
Jorissen, A., Začˇ, L., Udry, S., Lindgren, H.,& Musaev, F. A. 2005, A&A, 441, 1135
Karakas, A. I.,& Lattanzio C. J.,& Pols, O. R. 2002, PASA, 515, 19
Karakas, A. I.,& Lattanzio C. J. 2014, PASA, 31, 30
Karakas, A. I.,& Lugaro M. 2016, ApJS, 825, 26
Karakas, A. I. 2016, S.A.Lt, 229, 87
Karakas, A. I. 2018, MNRAS, submitted

Katz, D., Sartoretti, P., Cropper, M., Panuzzo, P., Seabroke, G. M., Viala, Y., Benson, K., Blomme, R., Jasniewicz, G., Jean-Antoine, A., Huckle, H., Smith, M., Baker, S., Crifo, F., Damerdji, Y., David, M., Dolding, C., Frémat, Y., Gosset, E., Guerrier, A., Guy, L. P., Haigron, R., Janßen, K., Marchal, O., Plum, G., Soubiran, C., Thévenin, F. ,Ajaj, M., Allende Prieto, C., Babusiaux, C., Boudreault, S., Chemin, L., Delle Luche, C., Fabre, C., Gueguen, A., Hambly, N. C., Lasne, Y., Meynadier, F., Pailler, F., Panem, C., Royer, F., Tauran, G., Zurbach, C., Zwitter, T., Arenou, F., Bossini, D., Gomez, A., Lemaitre, V., Leclerc, N., Morel, T., Munari, U., Turon, C., Vallenari, A.,& Žerjal, M. 2018

Kelson, D. D., Illingworth, G. D., van Dokkum, P. G.,& Franx, M. 2000, ApJ, 531, 159

Kupka, F., Piskunov, N., Ryabchikova, T. A., Stempels, H. C., & Weiss, W. W. 1999, A&AS, 138, 119

Lindegren, L., Hernandez, J., Bombrun, A., Klioner, S., Bastian, U., Ramos-Lerate, M., de Torres, A., Steidelmuller, H, Stephenson, C., Hobbs, D., Lammers, U., Biermann, M. ,Geyer, R., Hilger, T., Michalik, D., Stampa, U., McMillan, P. J., Castaneda, J., Clotet, M., Comoretto, G., Davidson, M., Fabricius, C., Gracia, G., Hambly, N. C., Hutton, A., Mora, A., Portell, J., van Leeuwen, F., Abbas, U., Abreu, A., Altmann, M., Andrei, A., Anglada, E., Balaguer-Nunez, L., Barache, C., Becciani, U., Bertone, S., Bianchi, L., Bouquillon, S., Bourda, G., Brusemeister, T., Bucciarelli, B., Busonero, D., Buzzi, R., Cancelliere, R., Carlucci, T., Charlot, P., Cheek, N., Crosta, M., Crowley, C., de Bruijne, J., de Felice, F., Drimmel, R. Esquej, P., Fienga, A., Fraile, E., Gai, M., Garralda, N., Gonzalez-Vidal, J. J., Guerra, R., Hauser, M., Hofmann, W., Holl, B., Jordan, S., Lattanzi, M. G., Lenhardt, H., Liao, S., Licata, E., Lister, T., Loffler, W., Marchant, J., Martin-Fleitas, J.-M., Messineo, R., Mignard, F., Morbidelli, R., Poggio, E., Riva, A., Rowell, N., Salguero, E., Sarasso, M., Sciacca, E., Siddiqui, H., Smart, R. L., Spagna, A., Steele, I., Taris, F., Torra, J., van Elteren, A., van Reeven, W.,& Vecchiato, A. 2018

Little-Marenin, I. R.,& Little, S. J. 1987, AJ, 93, 1539

Luck R. E.,& Bond, H. E. 1991, ApJS, 77, 515

Luck R. E.,& Heiter, U. 2007, AJ, 133, 2464

Luo, A. L., Bai, Z. R., et al. 2015, RAA, in press

Maiorca, E., Randich, S., Busso, M., Magrini, L., & Palmerini, S. 2011, ApJ, 736, 120

Malaney, R. A.,& Lambert, D. L. 1988, MNRAS, 235, 695

McClure, R. D. 1983, ApJ, 268, 264

McClure, R. D. 1997, PASP, 109, 536

Mennessier, M. O., Luri, X., Figueras, F., et al. 1997, A&A, 326, 722

Mishenina, T. V., Bienaymé, O., Gorbaneva, T. I.,& Charbonnel, C. 2006, A&A, 456, 1109

Miyamoto, M,& Nagai, R. 1975, PASJ, 27, 533

Navarro, J. F., Frenk, C. S.,& White, S. D. M. 1997, ApJ, 490, 493

Ness M., Hogg D. W., Rix H. W., Martig M., Pinsonneault M. H., Ho A. 2016, ApJ, 823, 114

Pereira, C. B., Sales Silva, J., A., Chavero, C., Roig, F.,& Jilinski E. 2011, A&A, 533, A51

Pourbaix, D., Tokovinin, A. A., Batten, A. H., Fekel, F. C., Hartkopf, W. I. et al. 2001,

Price-Whelan, A. M., Hogg, D. W., Johnston, K. V.,& Hendel, D. 2014, Apj, 4, 794

Price-Whelan, A. M. 2017, The Journal of Open Source Software, 2, 388

Sartoretti, P., Katz, D., Cropper, M., Panuzzo, P., Seabroke, G. M. ,Viala, Y., Benson, K., Blomme, R., Jasniewicz, G., Jean-Antoine, A., Huckle, H., Smith, M., Baker, S., Crifo, F., Damerdji, Y., David, M., Dolding, C., Fremat, Y., Gosset, E., Guerrier, A., Guy, L. P., Haigron, R., Janssen, K., Marchal, O., Plum, G., Soubiran, C., Thevenin, F., Ajaj, M., Allende Prieto, C., Babusiaux, C., Boudreault, S., Chemin, L., Delle Luche, C., Fabre, C., Gueguen, A., Hambly, N. C., Lasne, Y., Meynadier, F., Pailler, F., Panem, C., Riclet, F., Royer, F., Tauran, G., Zurbach, C., Zwitter, T., Arenou, F., Gomez, A., Lemaitre, V., Leclerc, N., Morel, T., Munari, U., Turon, C.,& Zerjal, M. 2018

Shectman, S. A.,& Johns, M. 2003, SPIE, 4837, 910

Schlafly, E. F.,& Finkbeiner, D. P. 2011, Apj, 737, 103

Smiljanic, R. 2012, MNRAS, 422, 1562

Smith, V. V.,& Wallerstein, G. 1983, ApJ, 273, 742

Smith, V. V. 1984, A&A, 132, 326

Sneden, C., Cowan, J. J., & Gallino, R. 2008, ARA&A, 46, 241

Takeda, Y., Sato, B. V.,& Murata, D. 2008, AJ, 60, 781

Travaglio, C., et al. 2001, ApJ, 549, 346

Webbink, R. F. 1986, In: Leung, K. C., Zhai, D. S.(eds.) Critical Observations versus Physical Models for Close Binary Systems. Gordon and Breach, New York, p.403

Whitelock, P. A., et al. 2013, MNRAS, 428, 2216

Valenti, J. A., & Piskunov, N. 1996, A&AS, 118, 595

Van Eck, S. & Jorissen, A. 1999, A&A, 345, 127

Van der Swaelmen, M., Boffin, H. M. J., Jorissen, A.,& Van Eck, S. 2017, A&A, 597, A68

This paper has been typeset from a TEX/LATEX file prepared by the author.